ISSN(Print) : 2320 -1967
ISSN(Online) : 2320 -1975

GLOBAL SCIENTIFIC INC.

ChemXpress

ORIGINAL ARTICLE

ChemXpress 7(1), 01-15, (2014)

Effect of the preparation method on carbon behavior and hydrogen selectivity during gasoline steam reforming over nano-Al_2O_3 catalysts

Dalia R.Abd El-Hafiz*, Mohamed A.Ebiad, Radwa A.El-Salamony

Egyptian Petroleum Research Institute, (EGYPT)
E-mail : dalia_epri@yahoo.com

Abstract : Hydrogen generation from gasoline is essentially one of the critical technologies for the commercialization of small-scale fuel cells auxiliary/backup power systems, so catalysts suitable for steam reforming of gasoline are desperately needed. So, in this work, the influence of metal type (Ni and Co) and preparation method (Co-precipitation and impregnation) on catalytic steam reforming of gasoline over nano-Al_2O_3 catalysts was studied at different reaction temperature (500-800°C). The structure and surface properties of the catalysts before and after reaction were tested by different characterization techniques such as TGA, XRD, TPR, HRTEM, BET surface areas and ramman spectroscopy. Results show that, the products distribution is dependent on both preparation method and metal type, on Ni/Al_2O_3 catalysts carbon product and methane is the major product, CO_2 and CO is much less than the value of H_2. The ratio of $CO_2/(CO+CO_2)$ represents the CO conversion (X_{CO}) for the WGS reaction, lower temperatures favor the WGS reaction on all of the prepared catalysts. On the other hand we can show that Ni catalysts favor WGS reaction more than that of Co catalyst. Although maximum H_2 selectivity (70%) is reached at 800°C over the Co/Al_2O_3 catalyst prepared by impregnation method, but when considering hydrogen production and carbon resistance at the same time, Ni/Al_2O_3 is most effective catalyst in gasoline steam reforming because it produced non-deactivating carbon. A higher thermal stability and graphitization degree of deposited carbon were obtained on Ni-Al_2O_3 and Co/Al_2O_3.

INTRODUCTION

The catalytic reforming of gasoline for the production of hydrogen on-board a vehicle is of general interest in the automotive industry. This is because among the primary fuels, gasoline has an existing infrastructure, a high power density and extensive public acceptance. In the same time, hydrogen can be cleanly and efficiently transformed into electricity power by application in full cell (FCs). The efficiency of a car with FC systems based on gasoline as fuel has two benefits; firstly, the energy efficiency of these cars will be higher than the efficiency of a car with an internal combustion engine. On the other hand, an electric motor associated with a fuel cell can eliminate the pollutants emissions such as NO_x produced from internal combustion engines.

The reforming processes for hydrogen production, either via steam reforming (SR), catalytic partial oxidation (CPO) or auto-thermal reforming (ATR) are perceived as the main commercially competitive methods to produce hydrogen from petroleum-based fuels[1,2]. SR provides the highest reforming efficiencies and H_2 yield; there have been several papers that discuss the advantage of hydrogen production by steam reforming of gasoline[3,4].

The current hydrocarbons steam reforming catalysts are mainly Ni/Al_2O_3 and Ni/MgO. These supports provide high crush strength and stability[5,6]. Some contradictory data has been reported about cobalt[7,8], compared with nickel, cobalt generally shows better behavior towards the suppression of carbon deposition and thus better stability under reaction conditions. The wide use of these systems as catalyst components prompted a renewed interest with regards to these materials in the form of nano-sized, high surface area powders. Recent investigations have shown that nanostructured Ni or Co-containing catalysts exhibit better catalytic activity and stability in reforming of methane compared to conventional Ni- or Co-containing ones[9-11]. Such metal based catalysts are either produced by impregnation or by co-precipitation of metal salts with the components of the “support”, both followed by calcination[12].

However, coking is a major problem associated with reforming of heavy hydrocarbon fuels such as gasoline over different catalysts. Literature[13-15] indicated that the oligomers formed on catalyst surface can be considered as the precursor of carbon deposition. It is well known that, the origin of carbon deposit could be different using different catalysts. Therefore, the aim of the present work is to study the performance of nanostructured Ni- and $Co-Al_2O_3$ catalysts prepared by different methods, and also to study the behavior of carbon deposit during gasoline steam reforming reaction. Coking formation behavior and mechanism during steam reforming of organic compound is a new question in our current research and the detailed study on carbon deposition mechanism will be carried out in the following research work.

EXPERIMENTAL

Catalyst preparation

(A) Impregnation method

Firstly, nano-sized porous gamma-alumina (γ-Al_2O_3) was prepared by control precipitation method[16]. In which (0.125M) ammonium bicarbonate ((NH_4HCO_3, 98%) (Merck)) and (0.066M) aluminium nitrate (($Al(NO_3)_3{\cdot}9H_2O$, 95%) (Merck)) solutions were added drop by drop from two separate burettes to a reaction vessel contain 400ml deionized water to precipitate Al cations in the form of hydroxides. The temperature was maintained at 70°C during control precipitation experiment. The pH was adjusted to ~ 10 using HNO_3 and/or NaOH (Merck, GR). The precipitate was aged at 70°C for 3h, filtered and re-dispersed again in hot 2 L of deionized water. The precipitate was finally filtered, washed thoroughly with warm deionized water and subsequently with ethanol followed by acetone, dried at room temperature then calcined in air at 550°C for 5 h to produce γ-Al_2O3 powders. Co/Al_2O_3 and Ni/Al_2O_3 samples were prepared by impregnating γ-Al_2O_3 support with aqueous solutions of $Co(NO_3)_2.6H_2O$ or $Ni(NO_3)_2.6H_2O$ respectively to produce 10% metal loading.

(B) Co-precipitation method

Likewise of γ-Al_2O_3 preparation method the Ni-Al_2O_3 sample were prepared by control precipitation method using a mixture of $Al(NO_3)_3.9H_2O$ and (0.066M) $Ni(NO_3)_2.6H_2O$.

Characterization methods

(A) Thermal gravimetric analysis (TGA)

Thermal gravimetric analysis (TGA) was carried out using SETARAM Labsys TG-DSC16 equipment in the temperature range from room temperature up to 1000°C under nitrogen flow, to follow the thermal stability of the prepared catalyst.

(B) X-ray diffraction analysis (XRD)

X-ray diffraction analysis (XRD) was carried out by Shimadzu XD-1 diffractometer using Cu-target&

Ni-filtered radiation, to trace the various changes in the crystalline structure and the different phases accompanied preparation method. Sample powders were packed in glass holder, during the measurement of the diffraction intensity by step scanning in 2θ range between 5 and 70°. The phase identification was made by comparing to the Joint Committee on Powder Diffraction Standards (JCPDS). The average crystallite size of the samples was determined from the XRD peaks using the Scherrer equation.

(C) High resolution transmission electron microscopy (HRTEM)

High resolution transmission electron microscopy (HRTEM) and energy dispersive X-ray (EDS) spectroscopy were conducted using a JEOL 2100F TEM at an accelerating voltage of 200 kV. To prepare the TEM samples, a dilute particle–ethanol colloidal mixture was ultrasonicated for 30 min and a drop of solution was placed on a carboncoated Cu TEM grid.

(D) The textural properties

The textural properties were determined from the N_2 adsorption-desorption isotherms measured at liquid nitrogen temperature (-196°C) using NOVA2000 gas sorption analyzer (Quantachrome Corporation) system. All samples were degassed at 200°C for 17h in nitrogen atmosphere prior to adsorption to ensure a dry clean surface. The adsorption isotherm was constructed as the volume adsorbed (Vcm^3g^{-1}) versus the equilibrium relative pressure P/P_o, where P is the equilibrium pressure and P_o is the saturated vapor pressure of nitrogen.

(E) Temperature programmed reduction (TPR)

Temperature programmed reduction (TPR) measurements were carried out to investigate the redox properties (the ease of reducibility of metal oxide) over the resultant materials. The experiments were performed in automatic equipment (Chem BET 3000, Quantachrome). Typically, 100mg of pre-calcined sample was loaded into a quartz reactor and pretreated by heating under inert atmosphere (20 ml/min nitrogen) at 200°C for 3h prior to running the TPR experiment, and then cooled down to room temperature in N_2. Then the sample was submitted to a constant rate of heat treatment (10°C/min up to 1000°C) in a gas flow (80ml/min) of the mixture hydrogen/nitrogen (5/95 vol%) as a reducing gas. A thermal conductivity detector (TCD) was employed to monitor the amount of hydrogen consumption.

(F) Raman spectra

Raman spectra were obtained at room temperature, using an HR UV 800 confocal scanning spectrometer (Horiba Jobin Yvon) equipped with a Peltier-cooled charge-coupled device (1152×298 pixels) for detection. The Raman scattering was excited using a 632.81nm excitation wavelength supplied by an internal He–Ne laser through an Olympus high-stability BXFM confocal microscope. Patterns were recorded in the 50–1000cm^{-1} Raman shift range with a spectral resolution of 0.5cm^{-1}. Lab SPEC v. 5 software was used for data acquisition and processing.

Catalytic activity

The steam reforming of gasoline was performed at atmospheric pressure in a continuous fixed bed down flow vertical tubular reactor[17]. 1 g of catalyst diluted with same sized quartz particles was used for catalytic tests. Prior to a run, the catalyst was reduced in situ at 500 °C for 2 h under a hydrogen flow rate of 20cm^3/min. Water/gasolin mixture (gasolin/H_2O = 1:8 mol/mol) premixed in a separate container was feed to evaporator (at 150°C) by a pump (Model RP-G6; FMI, USA) with flow rate 0.2ml/min. Nitrogen gas was fed into the evaporator with flow rate 40cm^3/min to uniformly carry the steam, the steam was then fed to the reactor. The reaction temperature was varied from 500 to 800°C.

The product stream was analyzed by use of two gas chromatographs (GC) (Agilent 6890 plus HP, Varian Natural Gas Analyzer type C model CP-3800). Selectivity values were calculated as the molar percentage of products obtained, excluding water; Selectivity of product = (mol of product/ total mol of H_2 and carbon-containing products in the outlet)*100.

RESULTS AND DISCUSSION

Catalyst characterization

(A) Thermal gravimetric analysis

The thermal behavior of the prepared samples was investigated using TGA and DTA from room temperature up to 1000°C (Figure 1). The curve shows an endothermic process and an exothermic one in parallel with two weight loss steps; an endothermic peak from 30 to 400°C corresponds to the loss of physically adsorbed water and the hydroxyl of the catalysts surface. A high temperature exothermic peak may be related to the crystallization and/or the weight loss due to components loss of the catalysts caused by certain reactions occurring at the high temperature[18]. From the whole weight loss process of catalysts, it can be seen that the curves of Ni/Al_2O_3 and Co/Al_2O_3 are almost the same, and their weight loss is higher than that of Ni-Al_2O_3.

(B) X-ray diffraction analysis

XRD patterns of the prepared catalysts are shown in Figure 2. Generally, the broad features of all diffractrograms were ascribed to the prepared nanostructured solids. For Ni-Al_2O_3 catalyst, only high intensity and broad diffraction peaks at $2\theta = 37.7, 44.56$ and 65.96° of $NiAl_2O_4$ (JCPDS 00-001-1299) are observed. No Bragg reflections detected for NiO, which suggests that, the co-precipitation method lead to the incorporation of small particle size NiO in Al_2O_3 structure to form the $NiAl_2O_4$ spinel phase[19].

In order to study the effect of preparation method on the phase structure, the XRD pattern of the Ni/Al_2O_3 prepared by the impregnation method was studied, the figure shows, peaks attributed to NiO phase at 2θ 43.29° and 62.77° (JCPDS 00-001-1258) in addition to that of Al_2O_3, this mainly due to the inhomogeneous distribution of the Ni species, thus the locations with NiO phase may exceed the limit of the $NiAl_2O_4$ formation[19]. Al_2O_3 and $NiAl_2O_4$ were difficult to be distinguishing by XRD due to peak broadening and superimposition, so the diffraction peaks enlarged from 60 to 70° to show the difference (Figure 2b). Moreover, the particle size of $NiAl_2O_4$ is smaller for Ni-Al_2O_3 (7.2 nm) catalyst than for Ni/Al_2O_3 (8.66 nm) as shown in TABLE 1.

It is noteworthy that, XRD pattern of Co/Al_2O_3 shows different peaks, peaks at 2θ 31.4°, 37° and 59.53° (JCPDS 00-001-1152) were ascribed to cubic Co_3O_4 crystallites[20], in addition to Al_2O_3 peaks. The increase in intensity and sharpness of Al_2O_3 peak at 37°, may be due the overlap with the peak assigned to the cubic Co_3O_4 crystallites. No diffraction peak of CoO, cobalt aluminate or other Co species were found as reported by Batista et al.[21]. The average crystal sizes of metals on catalyst surface were 17.9 nm for NiO and 26.32 nm for Co_3O_4 in Ni/Al_2O_3 and Co/Al_2O_3 respectively.

(C) High resolution transmission electron microscopy

The HRTEM photographs obtained from the prepared samples are shown in Figure 3. Analysis of the photographs for Ni-Al revealed particles with defined dimensions with slight contraction of the crystal lattice due to partial substitution of Al by Ni, having a grain size ranging from 2-4 nm. Although no separate NiO phases were discernible by the XRD of Ni-Al, STEM/EDS elemental mapping (not shown) identified nickel clusters, which indicate that, the co-precipitation method lead to incorporation of Ni inside the Al_2O_3 matrix. In Ni/Al and Co/Al systems, two phases are observed, corresponding to the presence of the Al_2O_3 in needle structure. While nickel oxide and cobalt oxide, present in crystalline structure as expected by XRD data. In the two later catalysts, the mean particle size is estimated to be in the range 10–14 nm and 18–22 nm respectively.

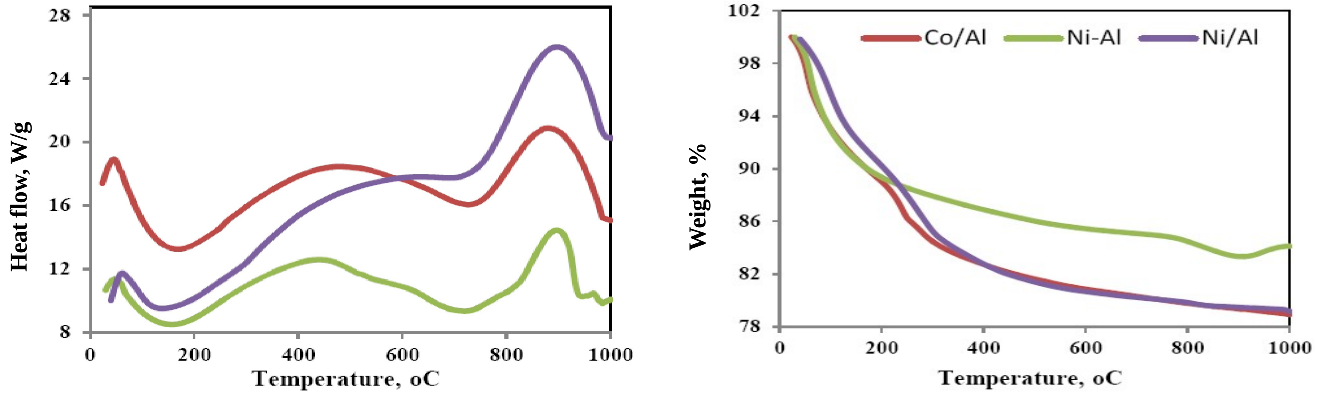

Figure 1 : TGA/DTA profiles of the prepared samples

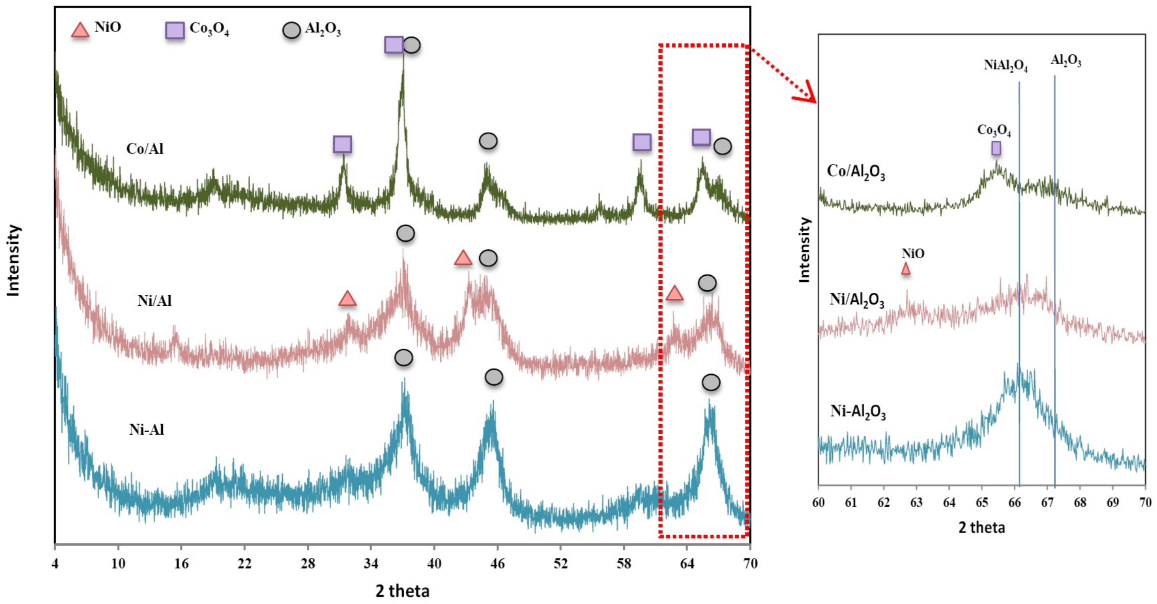

Figure 2 : XRD pattern for the prepared catalyst

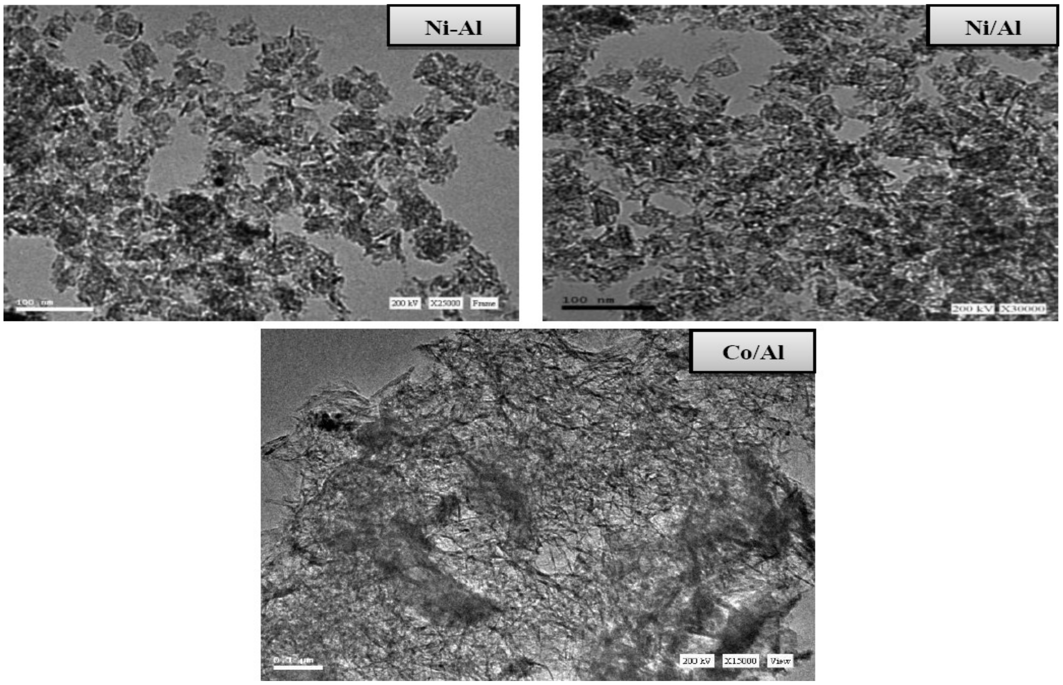

Figure 3 : TEM image of the prepared catalysts

(D) Surface areas

The nitrogen adsorption–desorption isotherms of the prepared samples are shown in Figure 4. Ni-Al sample exhibited IV-type isotherm with H2-type hysteresis loop, typical characteristics of mesoporous materials[22] as shown by BJH pore size distributions and T-plot represented in Figure 5, which retained well-developed framework mesopores with narrow pore size distributions centered at 4nm. While Ni/Al and Co/Al samples show type II isotherm with H3 hysteresis loop attributed to slit-shaped pores or plate-like particles with spaces between the parallel plates.

The values of specific BET surface area, together with the total pore volumes of the prepared samples are presented in TABLE 1. Compared with the Ni/Al_2O_3 prepared by impregnation method, Ni-Al_2O_3 catalyst shows much higher specific surface area and pore volume, this because in co-precipitation method, Ni species can be uniformly dispersed and reached to atomic or molecular level interaction with support. While in the case of impregnation method, the dispersion of nickel species could block part of pores on support and resulted in the lower specific surface. On the other hand, the impregnation by Co has little effect on the loss of surface area of Al_2O_3 (173.142m^2/g), this may be attributed the good dispersion of Co metal on alumina surface.

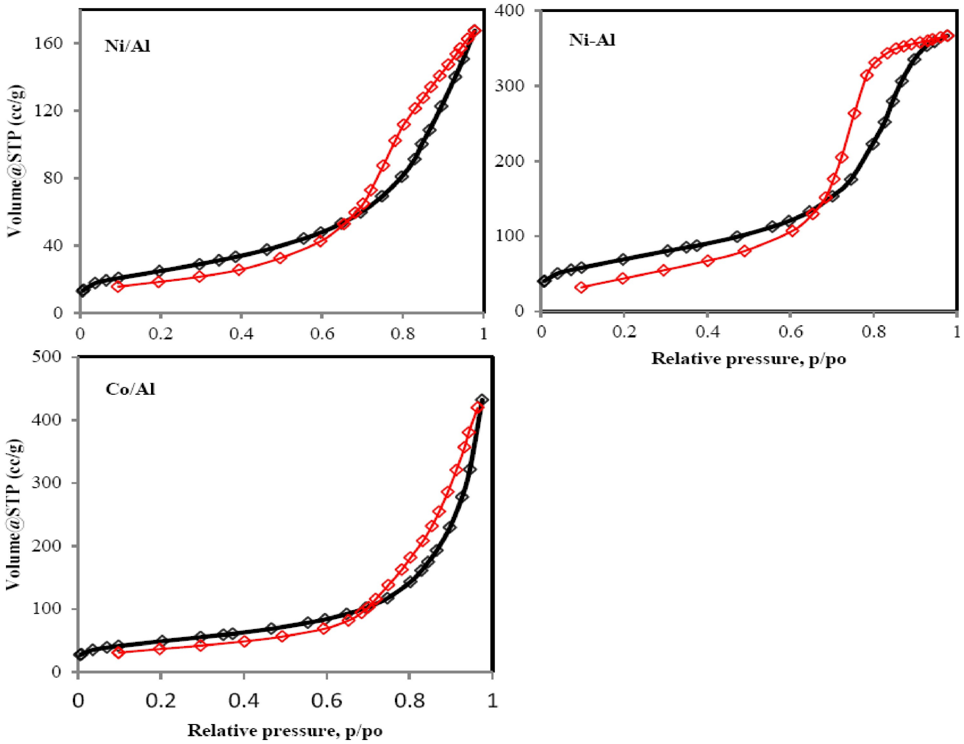

Figure 4 : Nitrogen adsorption–desorption isotherms of the prepared samples

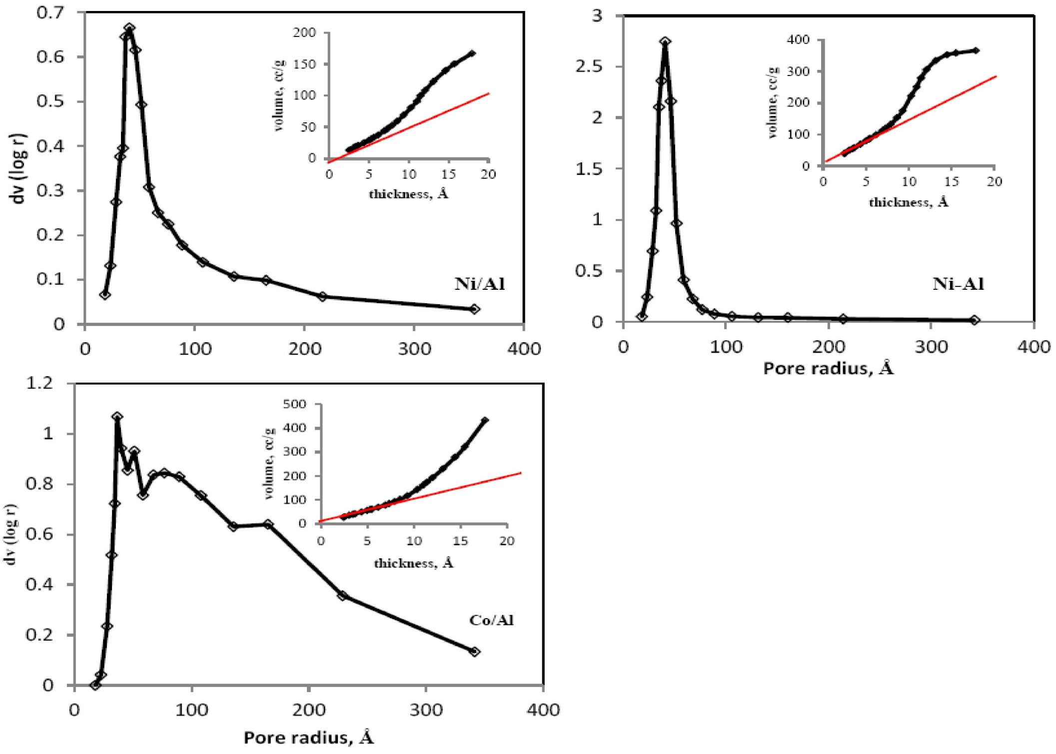

Figure 5 : Pore size distributions and T-plot of the prepared samples

TABLE 1 : Textural properties for the prepared Ni/CeO_2-ZrO_2

Catalyst	BET surface area m^2/g	Pore volume cm^3/g	Crystal size (metal) nm	Crystal size (support) nm
Ni-Al	249.158	0.5665	-	7.2
Ni/Al	90.939	0.2588	17.9	8.66
Co/Al	173.142	0.6679	26.32	9.73

(E) Temperature programmed reduction (TPR)

Continuing to the idea revealed by Chen, et. al.[23], about the strong metal-support interaction can effectively suppress the formation of deposited carbon; the TPR results obtain information about the effect of metal type and preparation method on metal-support interaction. The TPR profile for Ni-Al_2O_3 catalyst (Figure 6) has only one broad H_2 consumption peaks with a maximum at about 850°C, which mainly due to the reduction of NiO strongly interacted with the support by the formation of amorphous nickel aluminate spinel structure ($NiAl_2O_4$) as shown from XRD data[19]. This strong metal-support interaction can confine the agglomeration of the active metal and thus avoid metal sintering during the reaction.

While, the TPR curves for Ni/Al_2O_3 catalyst (Figure 6) showed different broad peaks (250-850°C) with three distinct regions of temperature. The weakest peak centered at about 304°C assigned to the reduction of free NiO. The second broad peak at 415°C was an indication of surface NiO species weakly interacting with the support[24,25]. The third peak, at about 712°C, related to reduction of the stoichiometric and non-stoichiometric nickel aluminate ($NiAl_2O_4$), which are more difficult to reduce[26]. Those different reduction temperatures were related to the inhomogeneous distribution of the Ni species in the Al_2O_3 support as confirmed by XRD data. So, the catalyst prepared by co-precipitation method show good Ni dispersion and difficult reduction degree than that prepared by impregnation method.

On the other hand, the TPR profile for Co/Al_2O_3 catalysts show two H_2 consumption peaks, reflecting a two-step reduction process ($Co_3O_4 \rightarrow CoO \rightarrow Co^0$), as previously described by Jacobs et al.[27]. The reduction of Co_3O_4 to CoO is achieved at 440°C, and the reduction of CoO to Co^0 occurs around 700°C (Figure 2A)[28]. Another small peak at about 840°C may be due to small amount of Co species that incorporated (strongly interacted) in the Al_2O_3 structure.

Catalytic activity

Akande et al.[29] investigated the effects of catalyst synthesis method, Ni loading, and temperature on the catalytic activity of Ni/Al_2O_3 catalysts for ethanol reforming. In their study, water/ethanol molar ratio of 13:1 was used, representing the actual composition of bio-ethanol produced by fermentation of biomass. Three

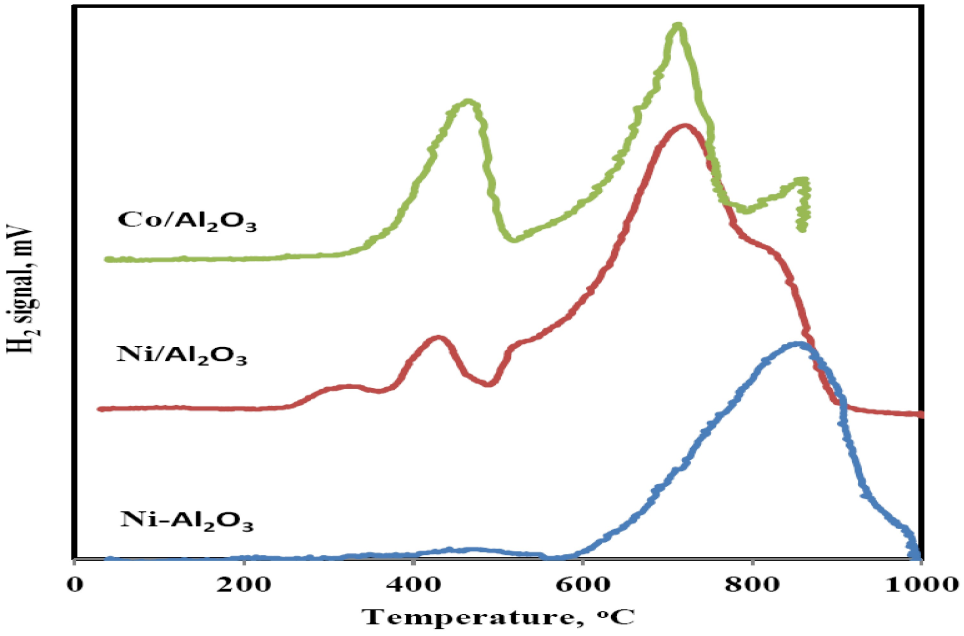

Figure 6 : TPR pattern of the prepared catalysts

types of preparation methods, namely, co-precipitation, precipitation, and impregnation, were evaluated. Optimal Ni loading of 15% was found for maximum ethanol conversion using Ni/Al_2O_3 catalyst prepared by co-precipitation and precipitation methods. For comparison, Ni loading did not show noticeable effect on Ni/Al_2O_3 activity when impregnation method was used. Regarding hydrogen production, the catalyst prepared by co-precipitation with Ni loading of 15% showed the best performance. In addition, Ni/Al_2O_3 prepared by co-precipitation also showed the highest selectivity of hydrogen.

Gasoline conversions and product selectivities for steam reforming on Ni-Al, Ni/Al and Co/Al catalysts are summarized in TABLE 2. To avoid the catalyst poisoning by sulfur, the used gasoline feed is the desulfurized gasoline fuel (~ 5 ppm sulfur). The main products of gasoline steam reforming are H_2, CH_4, CO, CO_2, C_2H_4, C_2H_6, C_3H_8, C_4H_{10}, C_5H_{12} and other heavy ends. Several reactions can occur during gasoline steam reforming depending on the reaction conditions[30], those reactions could be the Steam reforming reaction [Eq. (1)], Water gas shift reaction [Eq. (2)], Methanation of CO [Eq. (3)], Methanation of CO_2 [Eq. (4)] and by considering the reverse of reaction in Eq. (3), the steam reforming of methane is also considered in this reaction.

Steam reforming (SR):

$$C_nH_m + n\,H_2O \rightarrow n\,CO + (n+m/2)\,H_2 \tag{1}$$

Water gas shift (WGS):

$$CO + H_2O \rightarrow CO_2 + H_2 \tag{2}$$

Methanation of CO:

$$CO + 3H_2 \rightarrow CH_4 + H_2O \tag{3}$$

Methanation of CO_2:

$$CO_2 + 4H_2 \rightarrow CH_4 + 2H_2O \tag{4}$$

Figure 7 shows that, the higher carbon product (heavy ends) over all reaction temperature is lower on Co/Al_2O_3 than on Ni-Al_2O_3 than Ni/Al_2O_3, which indicates the higher catalytic activity of Co/Al_2O_3 catalyst in gasoline reforming at lower reaction temperature. The higher catalytic activity of Ni-Al_2O_3 than Ni/Al_2O_3, may be related to, in co-periciptation catalyst Ni species is much more homogeneously dispersed than that in impregnated one, which is helpful to obtain the small Ni particle sizes and then enhance the reaction efficiency in gasoline reforming.

The product distribution as a function of temperature on all catalysts is compared in Figures 8. Over all catalyst and over all temperature range the hydrogen and methane are the major products, while the CO and CO_2 exhibited the lowest selectivity.

The selectivity to H_2 was increase as the temperature increase over all catalyst to reach maximum value of 69.88% at 800°C over Co/Al catalyst. Therefore, it is effective to enhance the selectivity to H_2 by using Co instead of Ni as catalyst for gasoline steam reforming. On the other hand, the Ni-Al_2O_3 catalyst is more se-

TABLE 2 : Product distribution from GSR

Temp, °C	Product selectivity, mol %											
	Ni-AL_2O_3				Ni/AL_2O_3				Co/AL_2O_3			
	500	600	700	800	500	600	700	800	500	600	700	800
Hydrogen	0.82	15.24	20.28	49.75	10.82	13.11	19.22	36.48	23.64	29.58	44.40	69.88
Methane	8.16	29.54	48.55	45.25	9.16	17.03	30.97	37.09	65.44	67.29	39.85	10.15
CO	3.82	1.79	0.71	2.53	1.85	0.84	1.87	6.18	2.72	1.25	13.03	18.14
CO_2	2.35	0.57	0.30	0.50	1.38	4.86	2.89	1.57	1.14	0.33	0.97	0.59
Ethane	2.78	7.68	4.56	0.43	3.07	3.99	2.65	0.86	0.03	0.01	0.00	0.01
Ethylene	3.79	14.90	18.49	0.88	3.74	11.06	22.69	9.75	0.01	0.01	0.00	0.01
Propane	4.29	12.28	4.12	0.08	5.04	9.15	9.45	1.26	0.02	0.01	0.00	0.02
i-Butane	3.15	0.19	0.02	0.05	2.92	0.24	0.34	1.09	0.04	0.01	0.01	0.00
n-Butane	1.39	6.78	1.41	0.04	5.63	7.93	5.97	1.47	0.14	0.06	0.08	0.04
i-pentane	24.98	3.21	0.29	0.05	0.65	12.27	1.47	1.11	0.09	0.03	0.02	0.12
n-Pentane	8.40	1.34	0.13	0.02	15.79	4.71	0.62	0.59	0.06	0.02	0.01	0.06
Hexane & heavy end	36.07	6.48	1.15	0.42	39.97	14.80	1.85	2.54	6.67	1.41	1.62	0.98

lective to H_2 than Ni/Al_2O_3 catalyst due to the good Ni desperation in Ni-Al_2O_3 than in Ni/Al_2O_3 as shown by XRD data. So, we can clearly find that the product distribution for steam reforming of gasoline is dependent on both preparation method and metal type. Figure 9, show the value of H_2+CO over the prepared catalysts at all temperature range, from this figure we can show that the steam reforming reaction is favored over Co/Al_2O_3 catalyst than the other catalysts.

Although, at low temperature all catalyst are more selective to methane production and the Co catalyst exhibits more side product of methane than on the Ni one, as the temperature increase selectivity to methane was increase over Ni- catalyst and decrease over

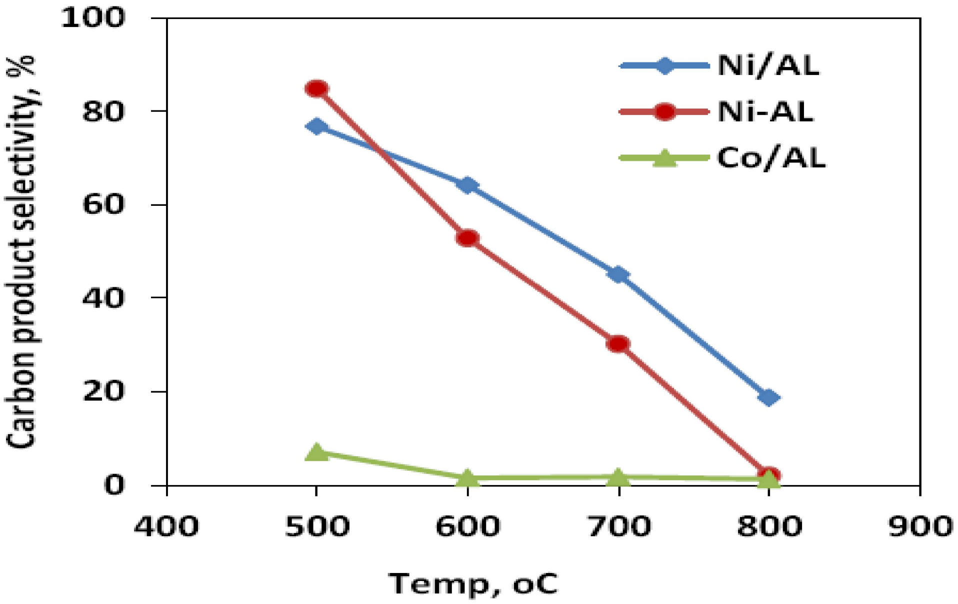

Figure 7 : Selectivity to carbon produced

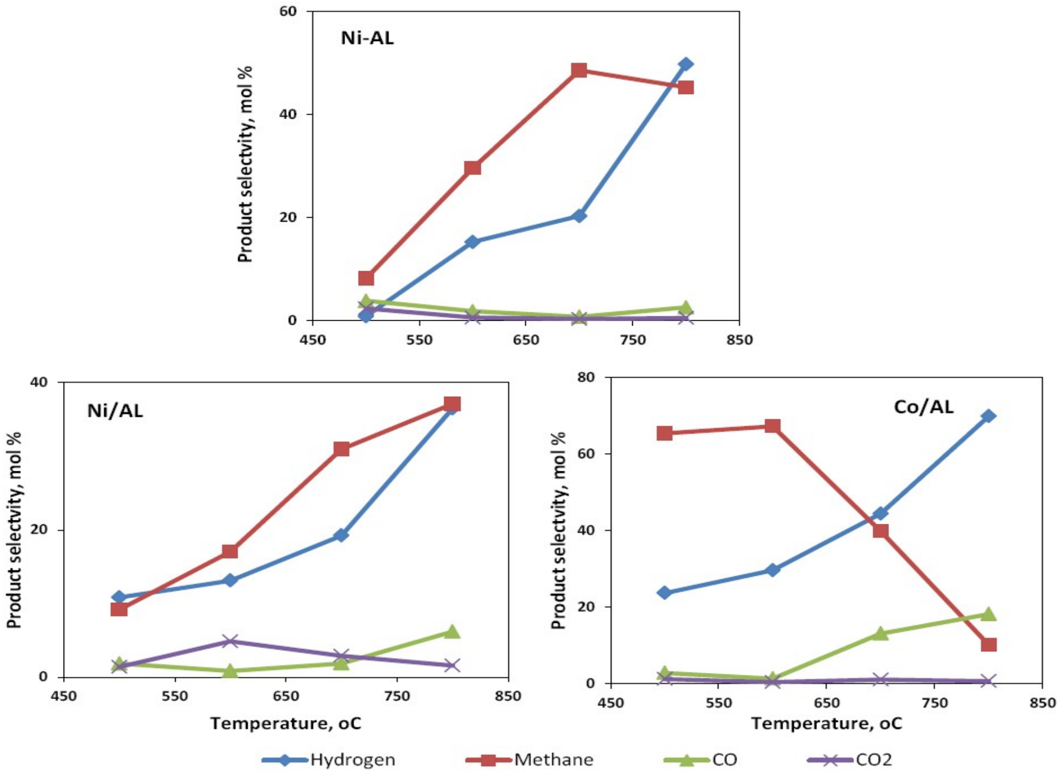

Figure 8 : Product distribution of gasoline steam reforming over the prepared catalysts

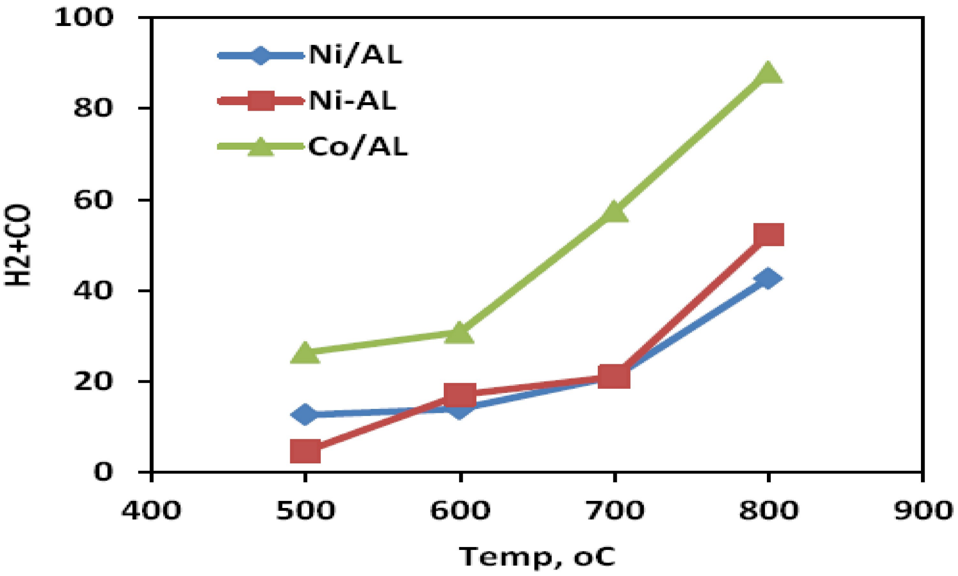

Figure 9 : H_2+CO over the prepared catalysts

Co-catalyst to reach the lower value 10.15% at 800°C. And Ni-Al_2O_3 produces methane more than Ni/Al_2O_3.

For conversion of CO to CO_2 and production of more hydrogen, a separated catalyst for water gas shift reaction is necessary. The water gas shift reaction proceeds as, $CO + H_2O = CO_2 + H_2$, the ratio of CO_2/($CO+CO_2$) represents the CO conversion for the WGS reaction. This ratio increases with decreasing temperature as shown in Figure 10. Therefore, lower temperatures favor the WGS reaction on all of the prepared catalysts. On the other hand we can show that Ni catalysts favor WGS reaction more than that of Co catalyst. This indicates that Ni/Al catalyst is active not only for steam reforming of gasoline to form hydrogen, but also for converting the CO into CO_2 by the water gas shift reaction. So in conclusion, hydrogen with high ratios of CO_2/($CO+CO_2$) is produced from gasoline by coupling reaction of steam reforming and water gas shift on Ni/Al_2O_3 catalyst at lower reaction temperature. This also explains why Ni/Al_2O_3 catalyst show high hydrogen yield at lower temperature than Ni-Al_2O_3 catalyst.

From the practical application point of view, high temperature operation was favorable for obtaining a better performance of Co/Al_2O_3 catalyst, when the temperature was higher than 600°C, the selectivity of hydrogen (H_2+CO) increased gradually with decrease of CH_4. Due to the reforming of CH_4 ($CH_4 + H_2O \rightarrow CO + 3H_2$) could produce more hydrogen. In addition, at high temperature, the steam reforming reaction to form CO and H_2 [Eq. (1)] was the dominating reaction whereas CO_2 was mainly produced as a secondary product by WGS reaction. While, Ni/Al_2O_3 catalyst can use as a secondary catalyst for conversion of CO to CO_2 and production of more hydrogen by WGS reaction.

Characterization of spent catalysts

It is well known that the stability of any catalysts depend on metal sintering, kind of deposited carbon and/or on location of the carbon on the catalyst surface. When carbon deposition occurred, the hydrocarbon can be adsorbed on catalyst surface and decomposed to carbon atom and carbonaceous atomic groups which can stay on catalyst surface and block metal atoms. Then the metal particle was forced to break away from the catalyst main body as the carbide grew. Finally, a carbide pillar formed. Carbon deposition can block the catalyst active center and micropore then lead to the decrease of catalytic activity. So, catalyst deactivation caused by carbon deposition is still the biggest bottleneck in steam reforming reaction. Therefore, it is necessary and significant to study the carbon deposition behavior.

(A) Thermo-gravimetric analysis

TABLE 3 shows the amount of carbon deposited per gram catalysts. Generally, the lower amount of carbon deposited over all of the prepared catalysts is mainly due to in steam reforming process, there is competition of carbon deposition and carbon elimination. So, high temperature and water feeding favor the carbon conversion from solid phase to gaseous phase[31]. Moreover, Ni/Al_2O_3 catalyst seems to show a better resistance to coke formation, or promoting the gasification of the carbon deposited on the catalyst surface, followed by Ni-Al_2O_3 and Co/Al_2O_3 catalysts. This result is greatly consistent with the catalytic activity toward CO_2 production, indicating that the current reactions (carbon gasification) primarily depend on the surface metal and also on the preparation methods.

TABLE 3 : The amount of carbon formed (g/g catalysts)

Catalysts	Weight loss (g/g catalysts)
Ni/Al_2O_3	0.3714
Ni-Al_2O_3	0.7646
Co/Al_2O_3	0.8488

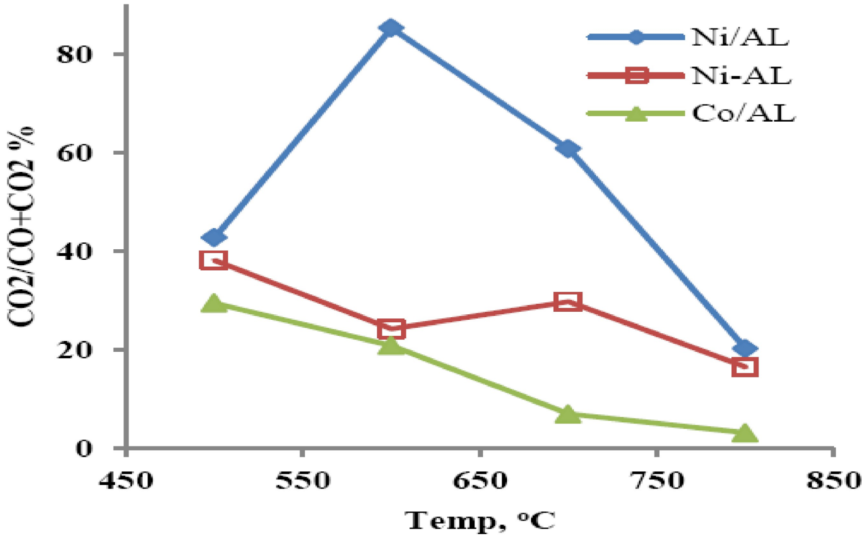

Figure 10 : Effect of reaction temperature on CO conversion (or WGSR)

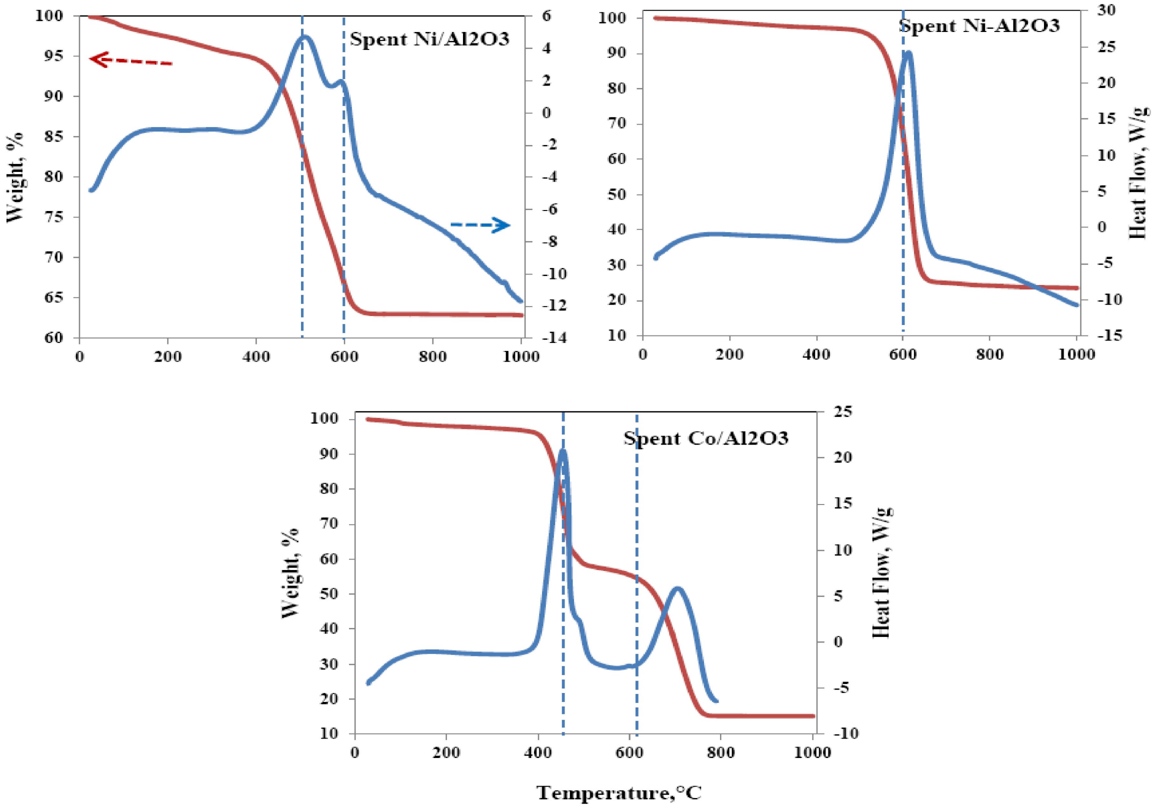

Figure 11 : TGA profile for nano-Al_2O_3 catalyst after 10h gasoline steam reforming

The carbon deposition state on catalyst surface can be in the form of nanofiber, but their concrete shapes can be different due to different catalyst. As shown in Figure 11, the three catalysts showed different behavior toward weight loss. A single step degradation was observed over Ni-Al$_2$O$_3$ catalyst at temperature above 600^{o}C indicating the deposition of carbon in the graphitic form[32,33] While, in case of Ni/Al$_2$O$_3$ most of carbon formed in the form of mono atomic carbon and filamentous coke (lower than 550^{o}C). The mono atomic carbon is highly reactive and can be easily oxidized at the surface of catalyst, while the deposited filamentous carbon is more stable at the surface of nickel and can oxidized at higher temperatures[34]. This indicates that the preparation of Ni-Al$_2$O$_3$ by co-precipitation method enhance the graphitization degree of the deposit carbon.

However, in Co/Al$_2$O$_3$ catalyst about 57.74% of deposited carbon was in the form of mono atomic carbon and filamentous coke (lower than 550^{o}C). And 42.26% of deposited carbon was carbon in the high graphitic form (higher than 600^{o}C), the higher oxidation temperature of this peak (700^{o}C) is due to the formation of carbon nano-fibers beside the CNTs[35], which is in a good agreement with the TEM data.

(B) Structural and textural parameters of the carbon

(a) X-ray diffraction analysis

Figure 12 shows the XRD pattern of spent catalysts after gasoline steam reforming. Ni-Al$_2$O$_3$ catalyst show strong peaks at 2Θ = 26.5^{o}, 42.9^{o} and 53.2^{o} representing the (002), (100) and (004) graphitic basal plane reflection in form of CNTs [ref. JCPDS card (00-058-1638)], the peak assigned NiAl$_2$O$_4$ was also observed. It is worth noting that, although the catalyst was reduced before reaction there isn't any peak assigned to the presence of Ni^0 metal was observed, this due to absence of free NiO in the fresh catalyst and the difficult reducibility of NiAl$_2$O$_4$ spinel under the reaction condition. Moreover, the graphitic carbon phase is prominent compared to the peaks of Al$_2$O$_3$ support.

For Ni/A$_2$O$_3$, NiAl$_2$O$_4$ was observed in addition to Ni^0 (at 2Θ reflections of 44.5^{o}, 51.7^{o}) and the peak attributed to NiO phase completely disappeared. The sharpness and high intensity of Ni^0 peaks may be indicating that, the Ni metal sintering unavoidable for this catalyst under the reaction conditions.

On the other hand, the small intensity of all peaks in Co/Al$_2$O$_3$ catalyst may be attributed to the coverage of the metal site by large amount of carbon deposited or the pillaring is formed.

(C) Raman of spent catalysts

Raman spectra in the high wavenumber region for the three spent catalysts are shown in Figure 13. All spectra had two bands, the first band is between 1200 and 1450 cm^{-1} (D-band) is associated to the disorder-induced vibration of C-C bond[36]. The second band is

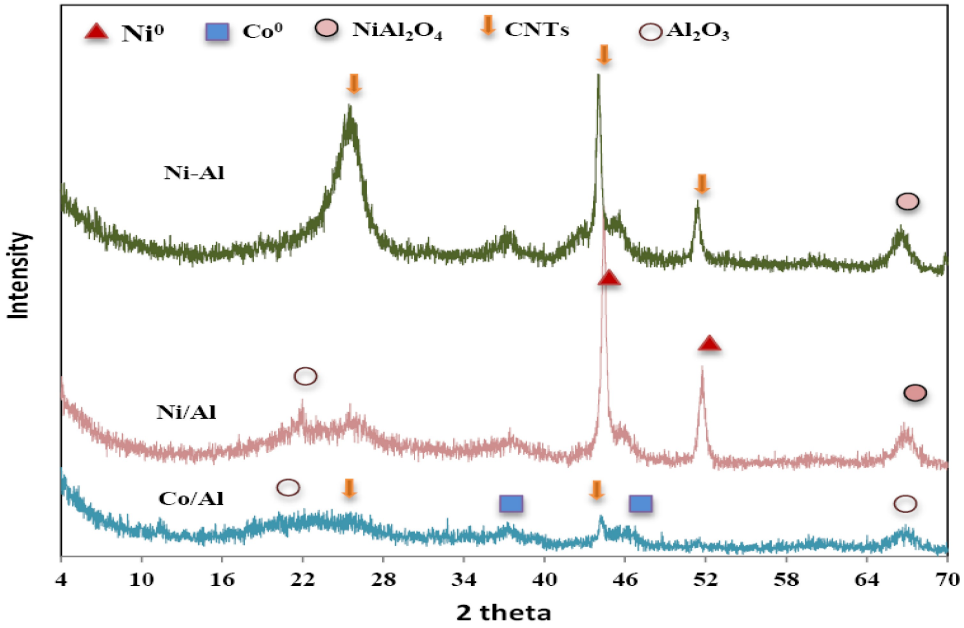

Figure 12 : XRD pattern for the spent catalysts

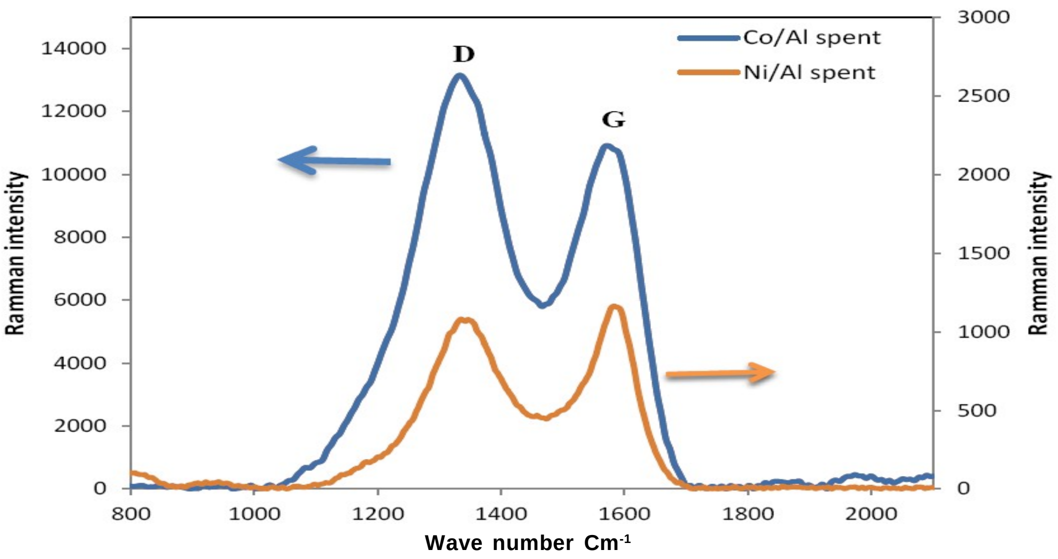

Figure 13 : Ramman spectra of the spent catalysts

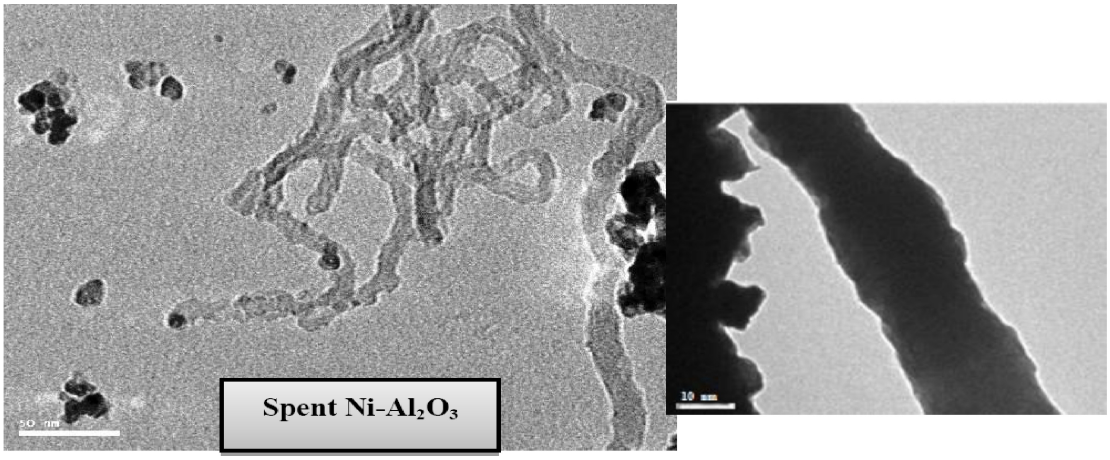

Figure 14 : TEM image of spent Ni-Al_2O_3 catalyst

between 1500 and 1700 cm^{-1} (G-band) is related to the C-C vibration of the carbon material with sp^2 orbital structure[37]. The G-band is a graphitic band produced by the high degree of symmetry and order of these graphitic carbon materials, it provides information about the electronic properties of the filamentous carbon and is used to identify well-ordered CNTs[38,39].

These findings suggest that the carbon species found on the surface of the catalysts tested in gasoline steam reforming consisted of deactivating (encapsulated carbon) and non-deactivating carbon (whisker carbon)[36,37], whose origins are diverse[40].

From Figure 13 we can noted that the intensities of the two bands were very high for Co/Al_2O_3 catalysts compared to Ni/Al_2O_3 one, and the intensity of the two bands were almost symmetric in Ni/Al_2O_3, which means that, in case Ni/Al_2O_3 the carbon filaments was coexisted with amorphous carbon. While, in case of Co/Al_2O_3, the high intensity of the D-band means that Co/Al_2O_3 lead to rapid activity loss due to more deposition of amorphous carbon, followed by a high selectivity for polymeric encapsulated carbon[41]. And the existence of small broad band at about 1750cm^{-1} (namely D/-band) suggested the presence of defective multi-walled carbon nanotubes (MCNT).

(D) High resolution transmission electron microscopy

The three catalysts were analyzed by TEM to gain a deeper insight into the type of carbon deposited on the surface. TEM images for Ni/Al_2O_3, Ni-Al_2O_3 and Co/Al_2O_3 catalysts after 10h of gasoline steam reforming reaction are presented in Figure 14. The catalysts show coke formation with different morphologies. The

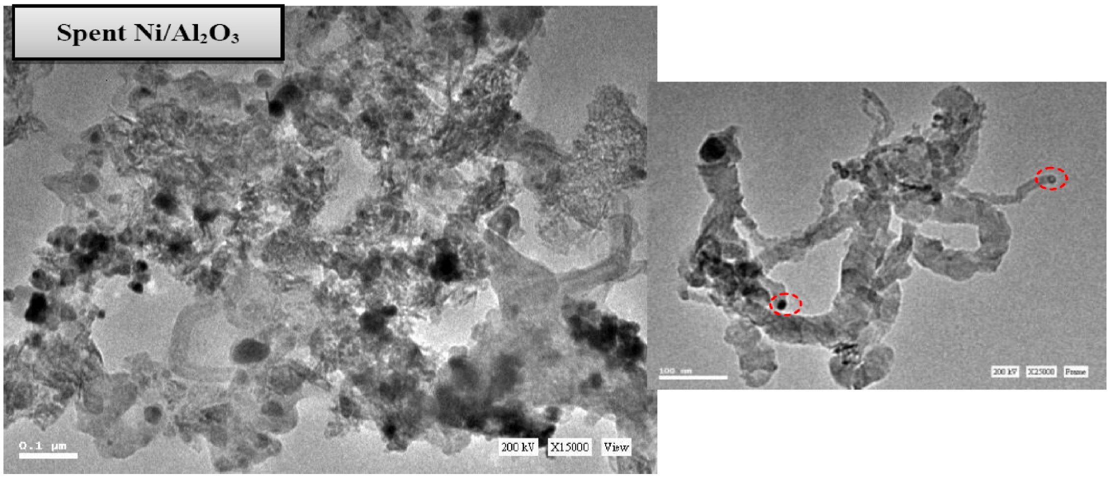

Figure 15 : TEM image of spent Ni/Al_2O_3 catalyst

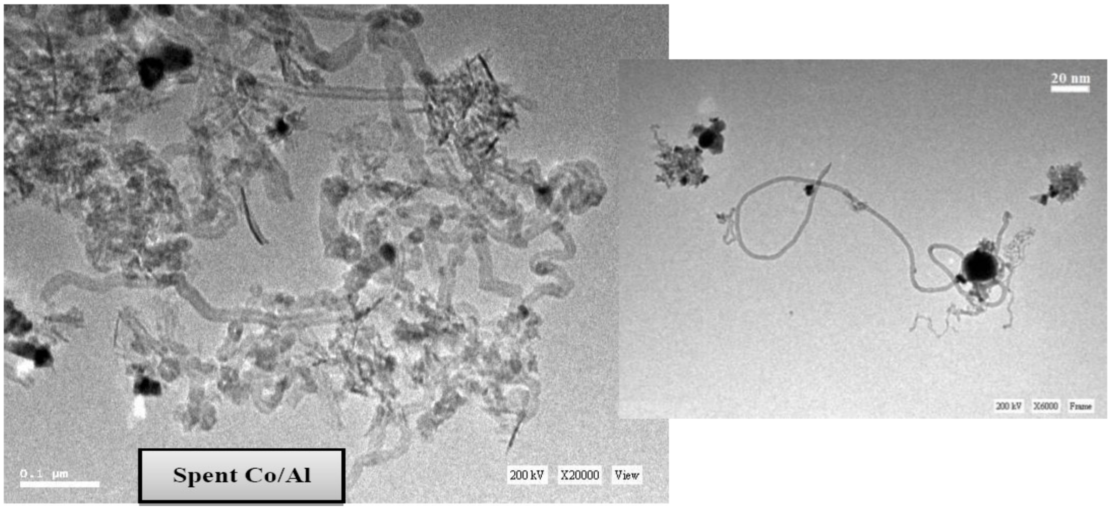

Figure 16 : TEM image of spent Co/Al_2O_3 catalyst

image of Ni-Al_2O_3 reveals that, the carbons are not concentric to the internal empty tube but rather opaque nano-rod. However, TEM images of the spent Ni/Al_2O_3 catalysts reveal the formation of amorphous carbon in addition to CNTs with Ni particles at the top of the tubes (indicated by the red circle in Figure 15). In the case of Co/Al_2O_3 catalyst (Figure 16), Web-like micrometre long CNTs partially covering the catalyst particle surface can be clearly observed. The figure also reveals the formation of carbon nano-fiber beside CNTs as confirmed by high oxidation temperature in thermal analysis data.

CONCLUSION

Preparation of Ni supported nano-alumina catalyst by co-precipitation method (Ni-Al_2O_3) exhibit high specific surface area, small Ni particle sizes, strong metal-support interaction and high Ni dispersion degrees, which make them an ideal material for catalytic steam reforming of gasoline with respect to that prepared by impregnation method (Ni/Al_2O_3). Ni-Al_2O_3 showed higher H_2/CO ratio and lower CO_2/CO+CO_2 ratio than the impregnation catalyst at all reaction temperature. Moreover, the use of Co instead of Ni shows most reactivity toward hydrogen production (highest H_2/CO and lowest CO_2/CO+CO_2). On the other hand, characterization of spent catalysts revealed that only limited graphitic carbon was found on the surface of the Ni-Al_2O_3 catalyst, and amorphous carbon (with mono atomic and filamentous morphology) covered most of the surface of the impregnation catalyst. The formation of Ni crystallites with $NiAl_2O_4$ is suggested to be an important factor in slowing Ni particle growth and coke formation. However, over Co/Al_2O_3 massive deposited carbon was in form of mono atomic carbon and filamentous coke while, small amount was graphitic carbon in form of carbon nano-fibers beside the CNTs.

REFERENCES

[1] P.K.Cheekatamarla, A.M.Lane; Int.J.Hydrogen Energy, **30**, 1277 **(2005)**.
[2] D.L.Hoang, S.H.Chan; Appl.Catal.A, **268**, 207 **(2004)**.
[3] A.Simson, R.Farrauto, M.Castaldi; Appl.Catal.B, **30**, 30 **(2011)**.
[4] L.Villegas, N.Guilhaume, H.Provendier, C.Daniel, F.Masset, C.Mirodatos; Appl.Catal.A, **281**, 75 **(2005)**.
[5] S.Gaur, D.J.Haynes, J.J.Spivey; Appl.Catal.A, **403**, 142 **(2011)**.
[6] O.Gamba, S.Moreno, R.Molina; Int.J.Hydrogen Energy, **36**, 1540 **(2011)**.
[7] V.M.G.Delacruz, R.P.Guez, F.Ternero, J.P.Holgado, A.Caballero; J.Phys.Chem.C, **116**, 2919 **(2012)**.
[8] D.S.J.Alonso, J.J.Juan, M.J.I.Gomez, M.C.R.Martınez; Appl.Catal.A, **371**, 54 **(2009)**.
[9] S.Therdthianwong, A.Therdthianwong, C.Siangchin, S.Yongprapat; Int.J.Hydrogen Energy, **33**, 991 **(2008)**.
[10] S.Jankhah, N.Abatzoglou, F.Gitzhofer; Int.J.Hydrogen Energy, **33**, 4769 **(2008)**.
[11] N.Wang, W.Chu, T.Zhang, X.-S.Zhao; Chem.Eng. J., **170**, 457 **(2011)**.
[12] G.Garbarinoa, S.Campodonicob, A.R.Pereza, M.M.Carnascialib, P.Rianib, E.Finocchioa, G.Buscaa; Appl.Catal.A, **452**, 163 **(2013)**.
[13] K.Takanabe, K.Aika, K.Inazu, T.Baba, K.Seshan, L.Lefferts; Journal of Catalysis, **243**, 263 **(2006)**.
[14] K.Takanabe, K.Aika, K.Seshan, L.Lefferts; Chemical Engineering Journal, **120**, 133 **(2006)**.
[15] B.Zhang, W.Cai, Y.Li, Y.Xu, W.Shen; Int.J.Hydrogen Energy, **33**, 4377 **(2008)**.
[16] K.M.Parida, A.C.Pradhan, J.Das, N.Sahu; Materials Chemistry and Physics, **113**, 244 **(2009)**.
[17] M.A.Ebiad, D.R.Abd El-Hafiz, R.A.Elsalamony, L.S.Mohamed; RSC Advances, **2**, 8145 **(2012)**.
[18] G.Xi-Kun, X.Ping-Ping, L.Shu-Dong; J.Fuel Chem.Technol., **36**, 732 **(2008)**.
[19] Z.Hao, Q.Zhu, Z.Jiang, B.Hou, H.Li; Fuel Processing Technology, **90**, 113 **(2009)**.
[20] R.Padilla, M.Benito, L.Rodrıguez, A.Serrano, G.Munoz, L.Daza; Int.J.Hydrogen Energy, **35**, 8921 **(2010)**.
[21] M.S.Batista, R.K.S.Santos, E.M.Assaf, J.M.Assaf, E.A.Ticianelli; J.Power Sources, **134**, 27 **(2004)**.
[22] J.G.Seo, M.H.Youn, I.K.Song; Int.J.Hydrogen Energy, **34**, 1809 **(2009)**.
[23] J.X.Chen, R.J.Wang, J.Y.Zhang, F.He, S.Han; Journal of Molecular Catalysis A, Chemical, **235**, 302 **(2005)**.
[24] S.B.Kwak, J.Kim, M.Kang; Int.J.Hydrogen Energy, **35**, 11843 **(2010)**.
[25] Y.Zhou, Q.Guo, M.Zhang, J.Yagi, L.H.Hatakeyama, J.Chen, M.Sakurai, H.Kameyama; Appl.Catal.A, **347**, 200 **(2008)**.
[26] F.F.de Sousa, H.S.A.de Sousa, A.C.Oliveira, M.C.C.Junior, A.P.Ayala, E.B.Barros, B.C.Viana, J.M.Filho, A.C.Oliveira; Int.J.Hydrogen Energy, **37**, 3201 **(2012)**.
[27] G.Jacobs, J.A.Chaney, P.M.Patterson, T.K.Das, B.H.Davis; Appl.Catal.A, **264**, 203 **(2004)**.
[28] G.Jacobs, B.H.Davis; Appl.Catal.A, **333**, 192 **(2007)**.
[29] A.J.Akande, R.O.Idem, A.K.Dalai; Appl.Cat.A, **287**, 159 **(2005)**.
[30] S.Rabe, F.Vogel, T.B.Truong, T.Shimazu, T.Wakasugi, H.Aoki, H.Sobukawa; Int.J.Hydrogen Energy, **34**, 8023 **(2009)**.
[31] C.Wu, R.Liu; Int.J.Hydrogen Energy, **35**, 7386 **(2010)**.
[32] L.Zhang, W.Li, J.Liu, C.Guo, Y.Wang, J.Zhang; Fuel, **88**, 511 **(2009)**.
[33] S.Freni, S.Carvallaro, N.Mondello, L.Spadaro, F.Frusteri; Catal.Commun., **4**, 259 **(2003)**.
[34] P.Wang, E.Tanabe, K.Ito, J.Jia, H.Morioka, T.Shishido, et al; Appl.Catal.A, **231**, 35 **(2002)**.
[35] A.E.Awadallah, A.A.Aboul-Enein, A.K.Aboul-Gheit; Renewable Energy, **57**, 671 **(2013)**.
[36] A.L.Pinheiro, A.N.Pinheiro, A.Valentini, J.M.Filho, F.F.Sousa, J.R.Sousa, M.G.C.Rocha, P.Bargiela, A.C.Oliveira; Catal.Commun., **11**, 11 **(2009)**.
[37] S.Damyanova, B.Pawelec, K.Arishtirova, M.V.Martinez Huerta, J.L.G.Fierro; Appl.Catal.B, **89**, 149 **(2009)**.
[38] M.S.Dresselhaus, G.Dresselhaus, A.Jorio, A.G.Souza Filho, R.Saito; Carbon, **40**, 2043 **(2002)**.
[39] C.Pan, Q.Bao; J.Mater Sci.Lett., **21**, 1927 **(2002)**.
[40] A.M.Amin, E.Croiset, W.Epling; Int.J.Hydrogen Energy, **36**, 2904 **(2011)**.
[41] F.F.de Sousa, H.S.A.de Sousa, A.C.Oliveira, M.C.C.Junior, A.P.Ayala, E.B.Barros, B.C.Viana, J.M.Filho, A.C.Oliveira; Int.J.Hydrogen Energy, **37**, 3201 **(2012)**.